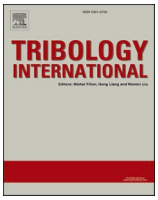
Tribology International 193 (2024) 109355



Contents lists available at ScienceDirect

Tribology International

journal homepage: www.elsevier.com/locate/triboint





Influence of V concentration in TiAlSiVN coating on self-lubrication, friction and tool wear during two-pass dry turning of austenitic steel 316 L

Ch Sateesh Kumar [a,b,*], Gorka Urbikain [a,b], Filipe Fernandes [c,d], Abbas AL Rjoub [c,e], Luis Norberto López De Lacalle [a,b]

[a] CFAA, Aeronautics Advanced Manufacturing Centre, University of the Basque Country (UPV/EHU), Biscay Science and Technology Park, Ed. 202, Zamudio, Spain
[b] Department of Mechanical Engineering, University of the Basque Country, Escuela Superior de Ingenieros Alameda de Urquijo S/N, 48013, Bilbao, Spain
[c] University of Coimbra, CEMMPRE, ARISE, Department of Mechanical Engineering, Rua Luís Reis Santos, 3030-788 Coimbra, Portugal
[d] ISEP, Polytechnic of Porto, Rua Dr. António Bernardino de Almeida, 4249-015 Porto, Portugal
[e] Department of Engineering Physics, Polytechnique Montréal, Montreal, Quebec H3T 1J4, Canada

ARTICLE INFO

Keywords:
Austenitic steel
TiAlSiVN
Self-lubricant coating
Machining

ABSTRACT

The present work investigates the performance of TiAlSiVN coating with 5 and 11 at% of V concentration deposited on the Al_2O_3/SiC cutting tools during dry turning of austenitic 316 L stainless steel. The maximum flank wear reduction compared to the uncoated tool for coated tools with 11% and 5% V concentration was 85% and 67%, respectively. The Raman analysis indicated the formation of V_2O_5 in the cutting zone, which helps to reduce friction and machining forces for the coated tools. Overall, the presence of higher V content (11 at%) enhances the self-lubrication behaviour of the TiAlSiVN coating, accounting to lower fluctuations in cutting forces, superior surface finish, and lower flank wear when compared to the TiAlSiV5N coated and uncoated cutting tools.

1. Introduction

The machinability of austenitic stainless steel has many challenges due to its low thermal conductivity and work hardening behaviour, leading to high machining forces and cutting temperatures, aggregated tool wear, and higher adhesion, causing built-up-edge formations [1,2]. However, austenitic stainless steel offers advantages such as superior corrosion resistance and high mechanical strength, making it suitable for different demanding applications [3]. One of the most prominent solutions for improving the machinability and cutting tool durability adopted during machining austenitic stainless steel is the use of cutting fluids, which would help reduce cutting temperatures and friction [4]. Although cutting fluids provide various advantages during machining, they are not sustainable at higher cutting temperatures [5–7]. They may be hazardous due to their non-biodegradable nature and generation of metal fumes at higher temperatures [8]. Further, the cutting fluids can change the machined surface's properties due to sudden temperature changes.

Thin-film depositions on the cutting tools have proved very effective in improving their performance by providing enhanced wear resistance, reduction in friction, and higher chemical and thermal stability [9–11]. It has been reported that the CVD and PVD coatings on cemented carbide inserts helped improve the durability of AISI 316 L austenitic steel cutting tools and simultaneously helped reduce material transfer and built-up-edge formations [12]. In addition, Das and Ghosh [3] revealed that a near-dry approach with a TiAlSiN nanocomposite coating deposited on carbide end mills effectively reduced tool wear during machining austenitic stainless steel. The TiAlSiN coatings, due to their enhanced oxidation resistance and superior hardness, are well suited for adverse machining conditions like high-speed machining [13,14]. Further, superior chemical stability at high temperatures makes it highly suitable for machining reactive materials [15] even under dry-cutting conditions [16].

The beneficial effect of coatings can be further improved by using novel self-lubricant coatings that generate lubricous phases during machining in the form of a tribolayer (TiO_2, V_2O_5, WO_3, etc.) [17–19] that could reduce friction at the chip-tool interface during machining. The vanadium-based self-lubricating coatings have recently gained popularity due to their rapid oxidation, leading to the generation of lubricous V_2O_5 in the cutting zone [20]. Further, TiAlSiN coating has

* Corresponding author at: CFAA, Aeronautics Advanced Manufacturing Centre, University of the Basque Country (UPV/EHU), Biscay Science and Technology Park, Ed. 202, Zamudio, Spain.
E-mail address: chigullasateesh.kumar@ehu.eus (C.S. Kumar).

https://doi.org/10.1016/j.triboint.2024.109355
Received 20 December 2023; Received in revised form 27 January 2024; Accepted 28 January 2024
Available online 2 February 2024
0301-679X/© 2024 The Author(s). Published by Elsevier Ltd. This is an open access article under the CC BY-NC license (http://creativecommons.org/licenses/by-nc/4.0/).

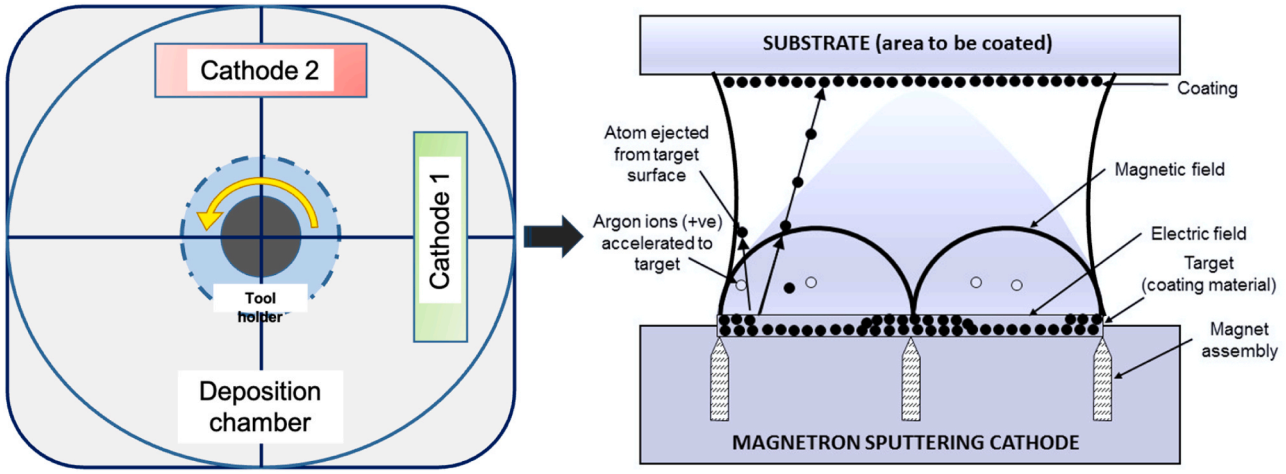


Fig. 1. Schematic representation of reactive magnetron sputtering setup.

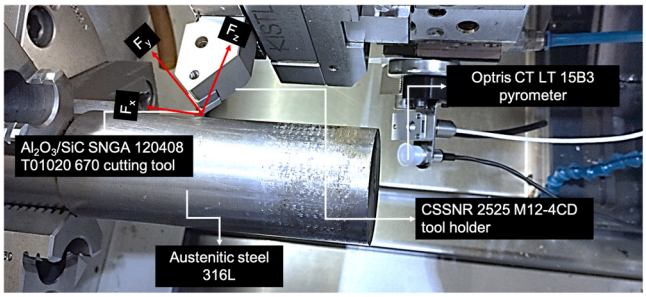


Fig. 2. Experimental setup for turning austenitic 316 L steel.

Table 1
Turning test conditions.

Cutting speed (m/min)	200	250	300	350
Depth of cut (mm)	0.5			
Feed rate (mm/rev)	0.1			
Cutting tools	Uncoated Al_2O_3/SiC		Al_2O_3/SiC tool with TiAlSiVN coating	

proved very effective during adverse machining conditions due to its high chemical and thermal stability, superior hardness, and enhanced wear resistance [21–24]. This behaviour can be attributed to the formation of nanocomposite structure with TiAlN acting as a reinforcement within the Si_3N_4 matrix, which leads to the development of a harder coating in comparison to TiAlN, AlTiN and AlCrN conventional commercial coatings [23–26]. However, their friction is significantly high, even when applying liquid lubrication. Al-Rjoub et al. [27] studied the influence of V additions on the morphology, structure and oxidation resistance of coatings as a tentative solution to produce self-lubricant coatings that could work without liquid lubrication. Oxidation results revealed the formation of a V2O5 phase on the surface of the coatings, which indicates the possibility of reducing friction in sliding contacts and avoiding the use of liquid lubrication.

The literature indicates that machinability and durability studies have not been performed on austenitic stainless steel with self-lubricating thin-film depositions on the cutting tools. Also, investigations on the application of novel TiAlSiVN coating have yet to be performed extensively. Thus, in the present work, the performance of TiAlSiVN coating will be studied during the dry turning of austenitic 316 L steel. Also, the effect of self-lubrication offered by the coating with varying V content will be investigated.

2. Methodology

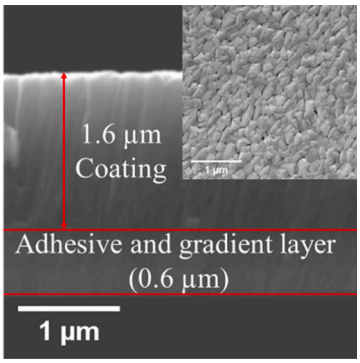
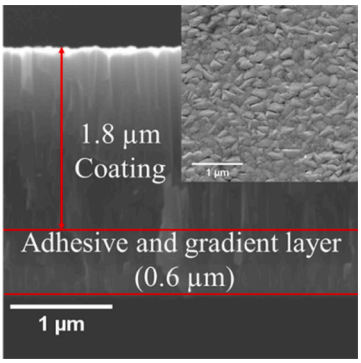
The experimental methodology involves the deposition of vanadium-based TiAlSiN coatings on the Al_2O_3/SiC whiskers reinforced mixed ceramic cutting tools. The machining performance was then performed in two passes to understand the performance of coatings more precisely. The detailed process has been elaborated below.

2.1. Coating deposition

The machining inserts were coated with TiAlSiVN films with 5 at% and 11 at% of V concentration using DC reactive magnetron sputtering system. The V concentration was selected considering the oxidation resistance of the coatings. Very high concentrations of V in the coating are not favourable since they lead to fast oxidation of the coatings and degradation of the mechanical properties. Further, very low V content, like 1–2%, would provide no beneficial effect since a limited amount of V-O phase is produced in the contact and consequently will not provide adequate lubrication. However, increasing V concentration reduced hardness and elastic modulus [27]. Thus, selecting a V concentration that is neither too low nor too high would be appropriate for investigating the effect of the amount of V in TiAlSiN coating during machining. Inside the chamber, there were two perpendicular cathodes with Ti and Cr targets (150 ×150 × 8 mm, purity (99.9%)). The 20 regularly spaced, 10 mm-diameter holes on the Ti target were filled with six Si and seven Al pellets, while the remaining holes were filled with three and six V-pellets to create two coatings with varying V concentrations.

The substrate holder, placed in the centre of the deposition chamber and vacuumed to an initial pressure of 3×10^{-4} Pa, held the machining inserts in place. After that, they were etched in an Ar environment for 40 min at a frequency of 250 kHz and a pulsed bias of − 230 V, while the two targets were shuttered and sputtered for 20 min. By delivering a power density of 5.3 W/cm^2 to the Cr target, regulating the deposition pressure to 0.3 Pa, and supplying a pulsed bias voltage of − 80 V to the substrate's holder for 5 min, a Cr adhesive interlayer was formed. Next, a gradient layer was deposited by gradually raising the N flow from 0 to 45 sccm for 5 min, gradually lowering the power provided to the Cr target until it was switched off, and applying a power density of 6.7 W/cm^2 to the Ti target. Pressure of final deposition was 0.5 Pa. The gradient layer was immediately followed by the final coats. All layers of the coatings were deposited in the rotation mode with a rotation speed of 20 rotations/min. The deposition time of the main coatings was fixed to 90 min. The schematic representation of the deposition setup is shown in Fig. 1. After the coating deposition, the coatings were characterized for adhesion, oxidation, Young's modulus, hardness, chemical composition,

Table 2
Surface morphology, cross-sectional morphology, chemical composition, and mechanical properties for TiAlSiVN coatings with varying V content.

Coating	TiAlSiV5N	TiAlSiV11N
Chemical composition (at%)	N- 47 Al-12 Si- 9 Ti- 27 V- 5	N- 45 Al- 11 Si- 9 Ti- 24 V- 11.0
Morphology (Cross section and Surface) As deposited		
Hardness (GPa)	32 ± 2	30 ± 2
Young's modulus (GPa)	306 ± 7	290 ± 13
Adhesion critical load Lc1 – first coating cracking (N)	50 ± 3	60 ± 2
Onset point of oxidation (°C)	720	640
Weight gain due to oxidation (mg/cm^2) at 700 °C for 30 min	0.15	0.17

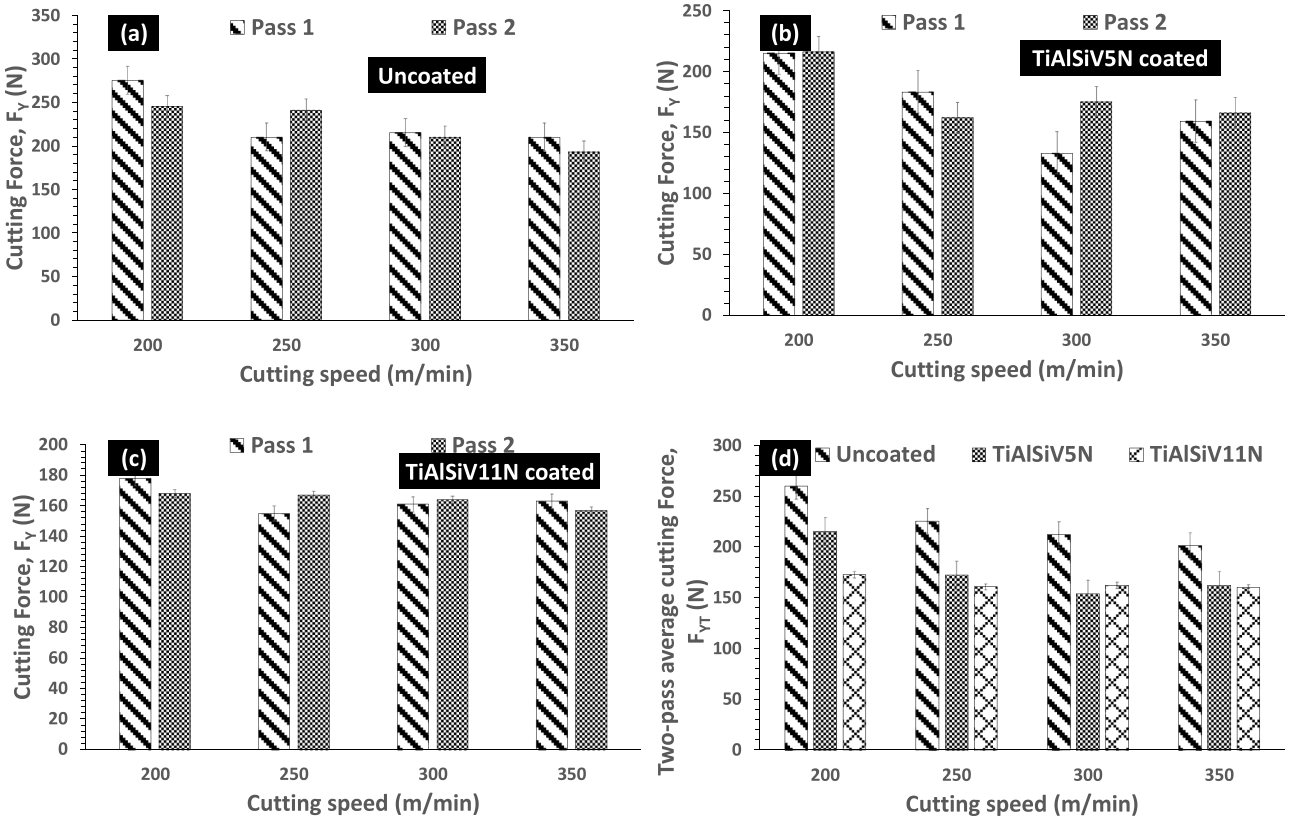


Fig. 3. Variation of cutting force with cutting speed for (a) Al_2O3/SiC uncoated, (b) TiAlSiV5N coated, and (c) TiAlSiV11N coated tools for two passes. (d) Variation of two-pass average cutting force with cutting speed.

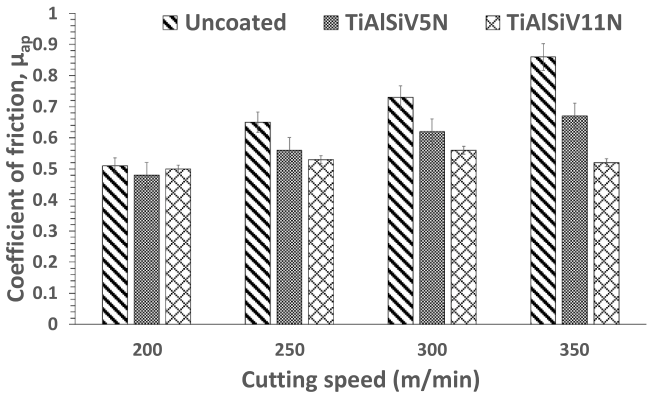


Fig. 4. Variation of coefficient of friction with cutting speed.

cross-sectional morphology, and surface morphology.

2.2. Turning tests

The turning tests were performed with uncoated, and TiAlSiVN-coated Al_2O_3/SiC tools with 5% and 11% vanadium content. The tests were performed in two passes under a dry cutting environment to understand the effect of V% on machining. Austenitic stainless steel with grade 316 L (Length: 500 mm and diameter 100 mm) was used as a workpiece for all cutting tests. Each pass involved a cutting length of 100 mm. The turning tests were repeated three times to maintain machining accuracy. The machining setup is shown in Fig. 2, whereas the machining conditions are listed in Table 1.

2.2.1. Measurement

During the cutting tests, the machining forces were measured using Kistler four-component piezoelectric dynamometer. The temperature measurements were also made during the cutting tests using an Optrics non-contact pyrometer with a resolution of 15:1 and measurement accuracy of ± 1° (CT LT 15B3 pyrometer). The pyrometer was pointed at the cutting tool near the tool-workpiece contact zone, and the temperature was recorded till the end of the cutting test. A mean was taken for evaluating a single average cutting temperature. The emissivity of the workpiece material has been set from the literature [28]. Although continuous measurements were made during tests, both forces and temperature measurements were averaged during each pass. After each pass, the surface roughness (R_A) was measured on the machined surface. The surface roughness measurements involved taking readings at ten different locations, and a mean value was taken to find the average surface roughness, which was used for comparison purposes. An optical microscope attached to the machine has been used to take the flank and crater wear images during the machining process.

2.2.2. Analysis

The measured machining forces were used to calculate the coefficient of friction as per the equation elaborated by Özel [29].

$$\mu_{ap} = \frac{F}{R} \quad (1)$$

Where

$$F = F_{xz} + F_y \tan\alpha \quad (2)$$

$$R = F_y - F_{xz} \tan\alpha \quad (3)$$

$$F_{xz} = \sqrt{F_x^2 + F_z^2} \quad (4)$$

In Eqs. (2–4), Fy represents cutting force, Fx represents feed force, Fz represents thrust force, Fxz represents equivalent thrust force, and α

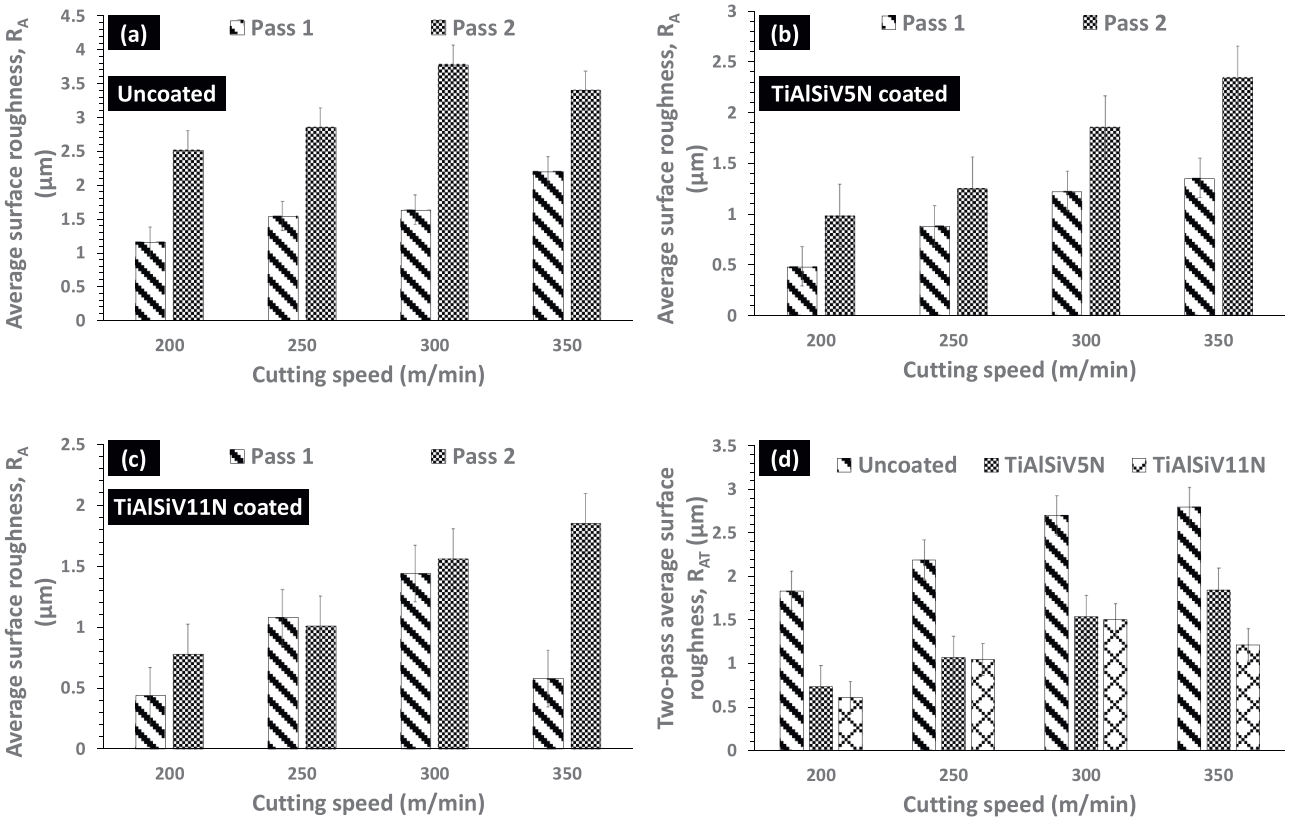


Fig. 5. Variation of surface roughness with cutting speed for (a) Al_2O_3/SiC uncoated, (b) TiAlSiV5N coated, and (c) TiAlSiV11N coated tools for two passes. (d) Variation of two-pass average surface roughness with cutting speed.

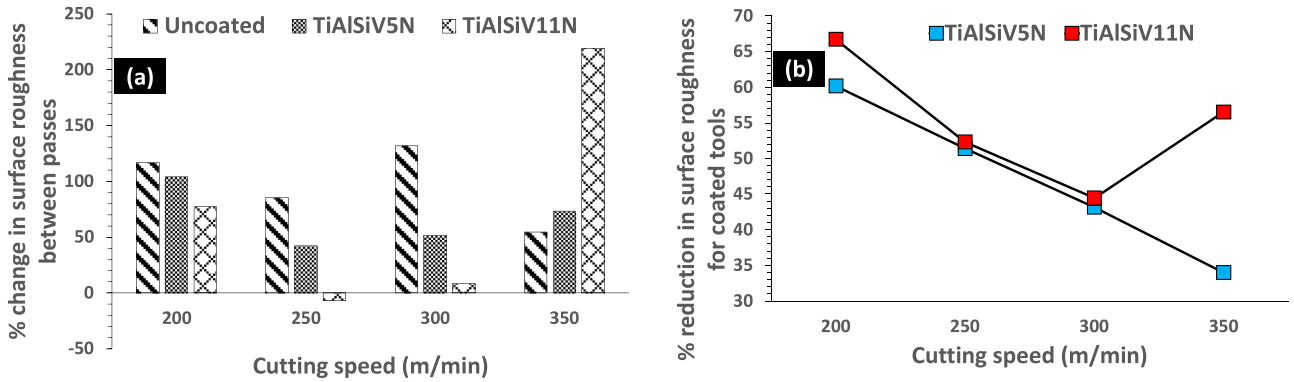


Fig. 6. Variation with cutting speed in (a) percentage (%) change in surface roughness between passes and (b) percentage (%) reduction in surface roughness for coated tools.

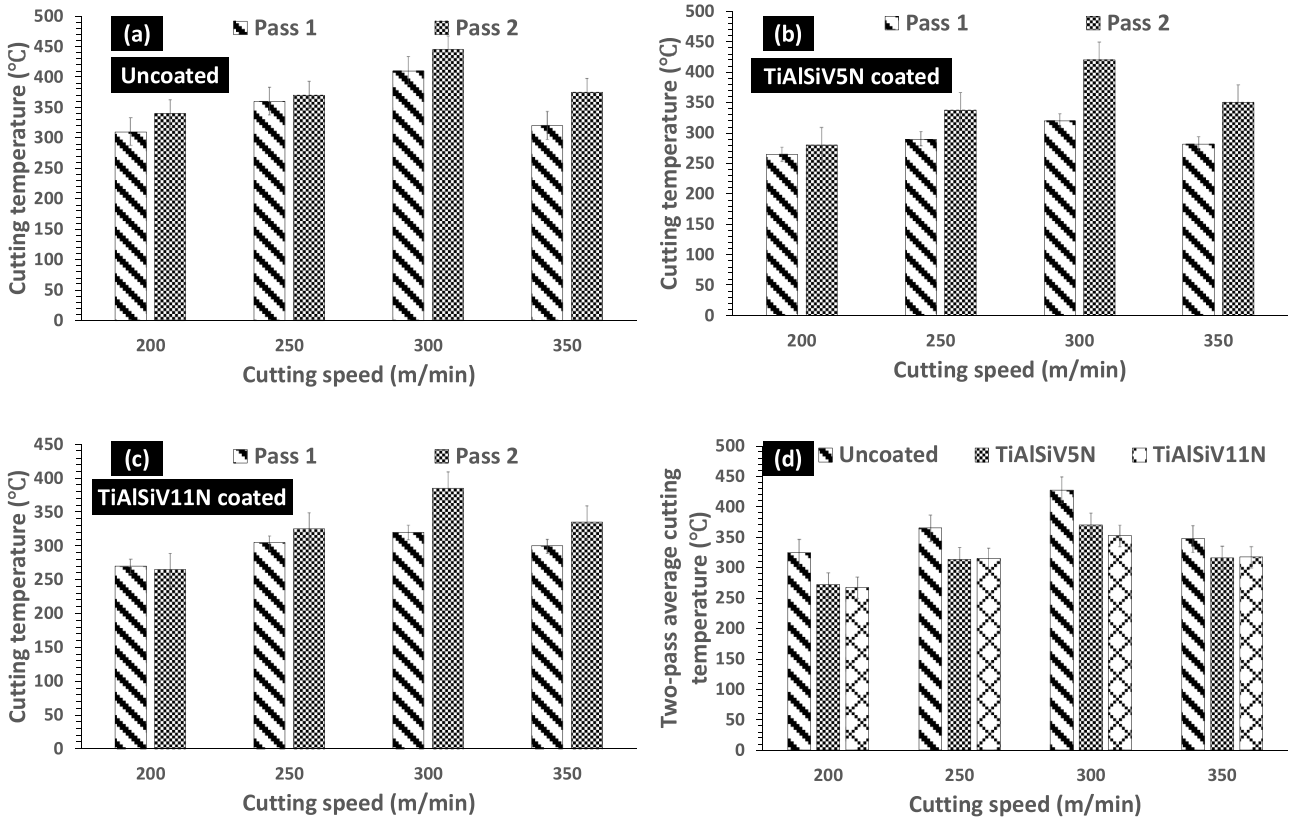


Fig. 7. Variation of cutting temperature with cutting speed for (a) Al_2O_3/SiC uncoated, (b) TiAlSiV5N coated, and (c) TiAlSiV11N coated tools for two passes. (d) Variation of two-pass average cutting temperature with cutting speed.

represents orthogonal rake angle. An orthogonal friction calculation system has been used as an oblique cutting system is more complicated to evaluate. Further, the difference in calculated friction coefficients remains 5–6% with the same trend for orthogonal and oblique calculations [30]. Tool wear behaviour was investigated using scanning electron microscopy (SEM). Energy dispersive spectroscopy (EDS) has been used to study material adhesion and elemental mapping on the wear zones. Raman spectroscopy has been used to identify the oxides in the adhesion zones on the TiAlSiVN coated and uncoated cutting tools.

3. Results and discussions

3.1. Structure, mechanical properties, and oxidation behaviour

Prior to the machining tests, the coatings deposited on the cutting tools were characterized for structure, mechanical properties, coating/substrate adhesion strength, and oxidation behaviour. As presented in Table 2, the coatings displayed a sub-stoichiometric composition since the metallic-to-N element ratio (Ti +Al + Si + V)/N is higher than 1. The TiAlSiV5N coating exhibits higher values of H and E than TiAlSiV11N, due to the pronounced substitutional solid solution effect, of V in the fcc lattice occurred in the former coating. The columnar morphology of both coatings was dense and compact, reaching from the adhesive interlayer to the coating's upper surface. The coating's adhesion at 11% V concentration was found to be somewhat better than that of the coating at lower V concentrations. As the V content rises from 5 to 11 at %, the coating's oxidation resistance and onset point both deteriorate. The rapid V diffusion to the surface, which prevents the creation of protective oxide layers, is what causes this deterioration. V-O-rich phases occur on top of the oxide layer.

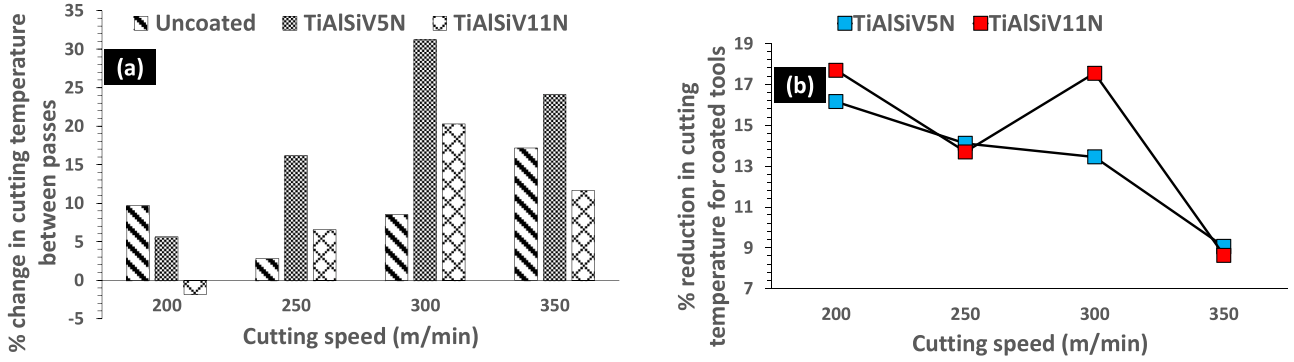


Fig. 8. Variation with cutting speed in (a) percentage (%) change in cutting temperature between passes and (b) percentage (%) reduction in cutting temperature for coated tools.

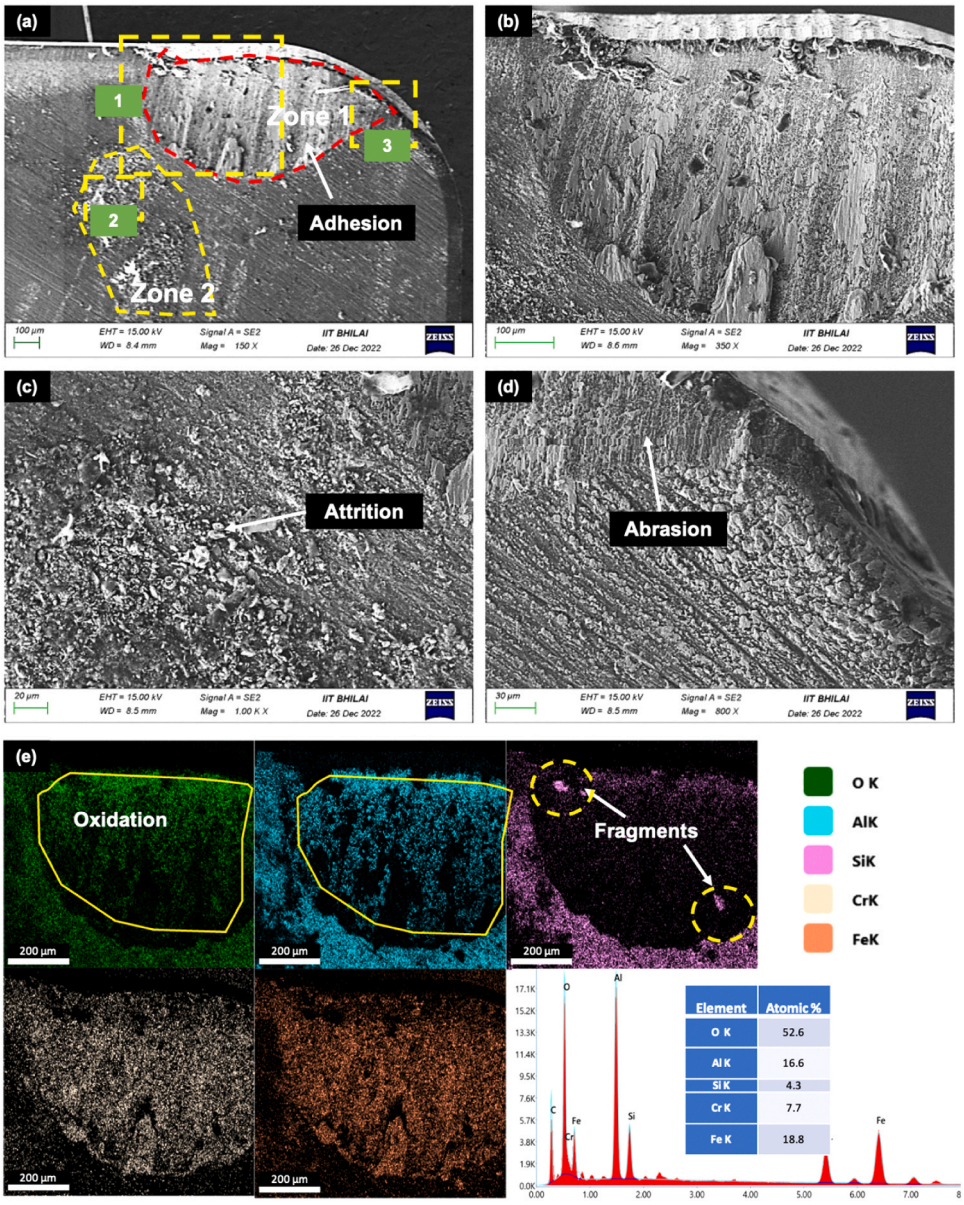


Fig. 9. (a) SEM micrographs showing wear on the rake surface of Al_2O_3/SiC uncoated tool after machining at 350 m/min cutting speed (b) magnified SEM image of marked region 1 in Fig. 9(a), (c) magnified SEM image of marked region 2 in Fig. 9(a), (d) magnified SEM image of marked region 3 in Fig. 9(a) and (e) EDS elemental mapping of the cutting zone for Al_2O_3/SiC uncoated tool.

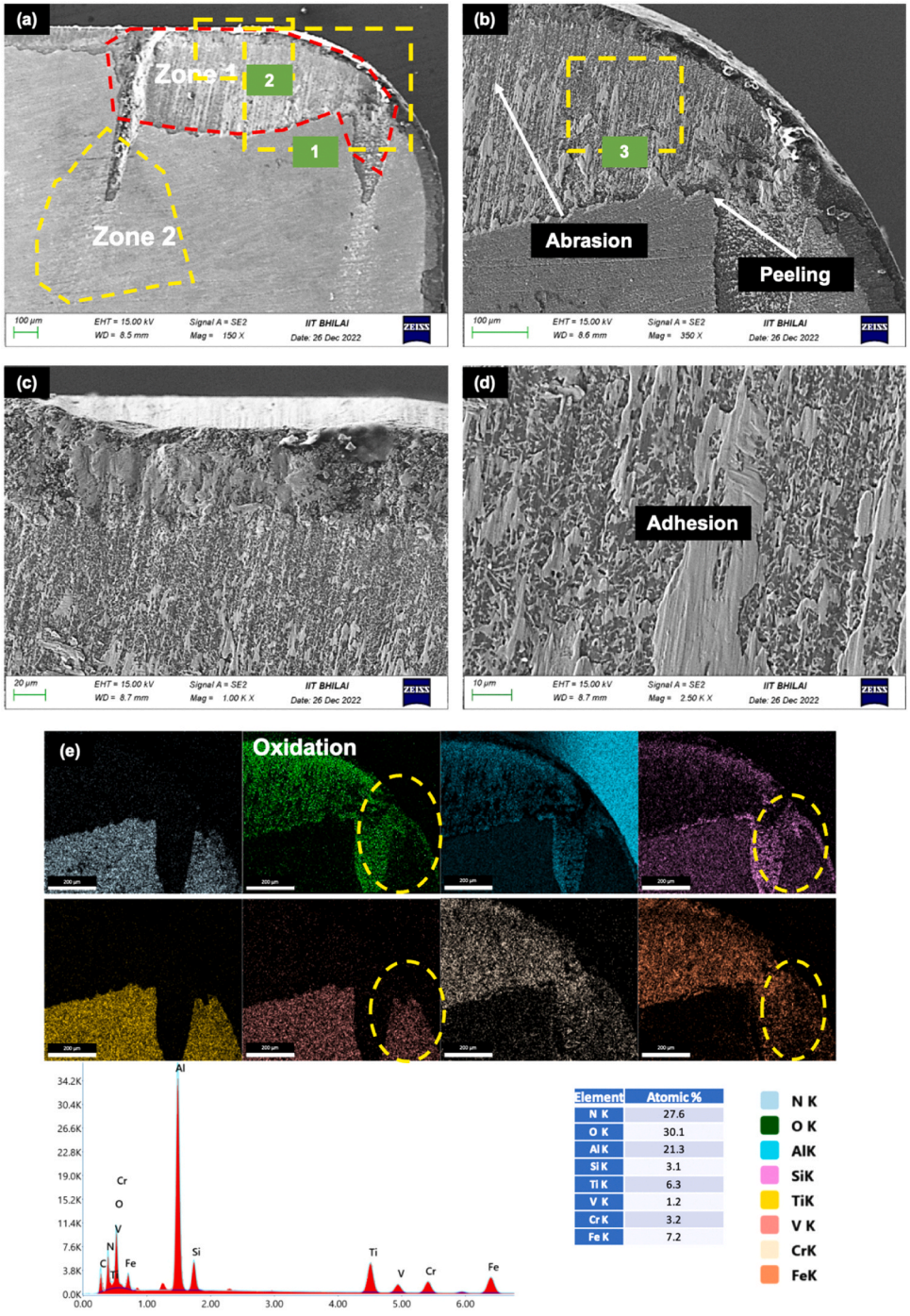


Fig. 10. (a) SEM micrographs showing wear on the rake surface of TiAlSiV5N coated tool after machining at 350 m/min cutting speed, (b) magnified SEM image of marked region 1 in Fig. 10(a), (c) magnified SEM image of marked region 2 in Fig. 10(a), (d) magnified SEM image of marked region 3 in Fig. 10(b) and (e) EDS elemental mapping of the cutting zone for TiAlSiV5N coated tool.

3.2. Forces and friction

Fig. 3 shows the variation of cutting force with cutting speed for TiAlSiV5N and TiAlSiV11N coated, and uncoated cutting tools. Also, in Fig. 3(a), (b) and (c) variation of cutting forces are shown with each pass. The cutting force reduces with increase of cutting speed which may be due to thermal softening of the workpiece [31], induced by growth in chip sliding velocity with cutting speed [32]. The two-pass machining used in the present work does not necessarily affect the cutting force and they remain within the deviation range. Interestingly, the decrease in cutting forces for the TiAlSiV11N coated tool is minimal with cutting speed. Also, the deviation in cutting forces is minimum during machining with TiAlSiV11N coated tool. Both the TiAlSiV5N and TiAlSiV11N coated tools showed significant reduction in two-pass average cutting force (F_{YT}) (a maximum of 27% for TiAlSiV5N and 34% for TiAlSiV11N coated tools) in comparison to the uncoated cutting tool (see Fig. 3(d)). This reduction can be due to the lower tool wear for coated tools. Also, generation of lubricious phases of V, such asV_2O_5 can be the reason for reduced machining forces as suggested Kumar et al. [18]. This phenomenon will be later elaborated through SEM and Raman analysis. In this regard, Fig. 4 shows the variation of coefficient of friction (μ_{ap}) with cutting speed. It is evident from the results that the

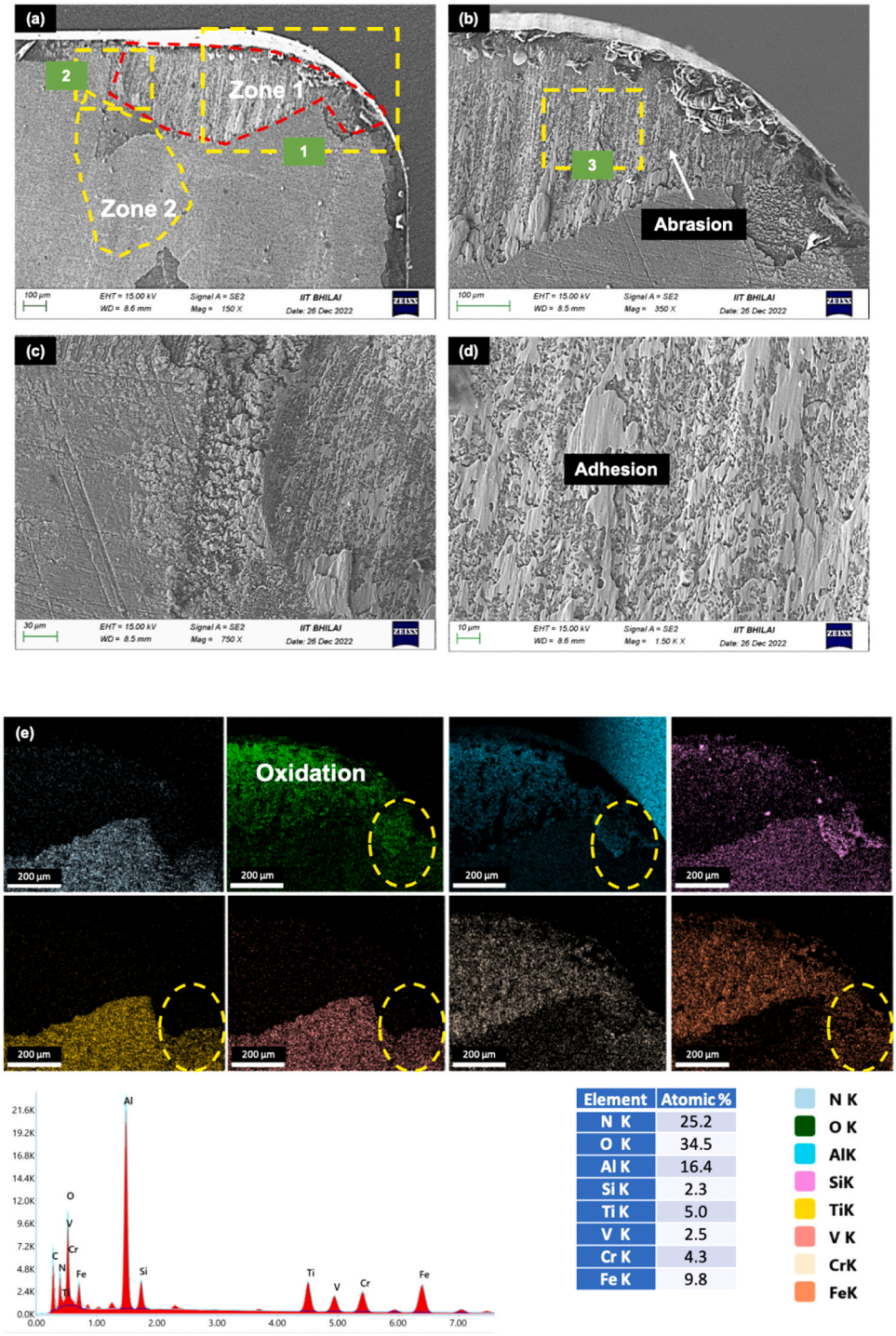


Fig. 11. (a) SEM micrograph showing wear on the rake surface of TiAlSiV11N coated tool after machining at 350 m/min cutting speed, (b) magnified SEM image of marked region 1 in Fig. 11(a), (c) magnified SEM image of marked region 2 in Fig. 11(a), (d) magnified SEM image of marked region 3 in Fig. 11(b) and (e) EDS elemental mapping of the cutting zone for TiAlSiV11N coated tool.

coated tools help in reducing the apparent friction at the chip-tool interface with TiAlSiV11N tool showing maximum reduction. Also, an increase in frictional coefficient can be seen with cutting speed indicating increase of tool wear with cutting speed.

3.3. Surface roughness

Fig. 5 shows the variation of average surface roughness with cutting speed. Also, the surface roughness has been measured after each pass and has been plotted against cutting speed in Fig. 5(a), (b), and (c) for uncoated, TiAlSiV5N coated, and TiAlSiV11N coated cutting tools respectively. It is observed that the surface roughness always increases for the second pass indicating progressive increase of tool wear. On the contrary, TiAlSiV11N coated tool showed minimal change in surface roughness for the second pass till 300 m/min cutting speed. However, a significant rise in surface roughness in the second pass is seen at 350 m/min demonstrating loss of beneficial effect of lubrication offered by the coating (see Fig. 6(a)). Nevertheless, when the two-pass average (R_{AT}) is

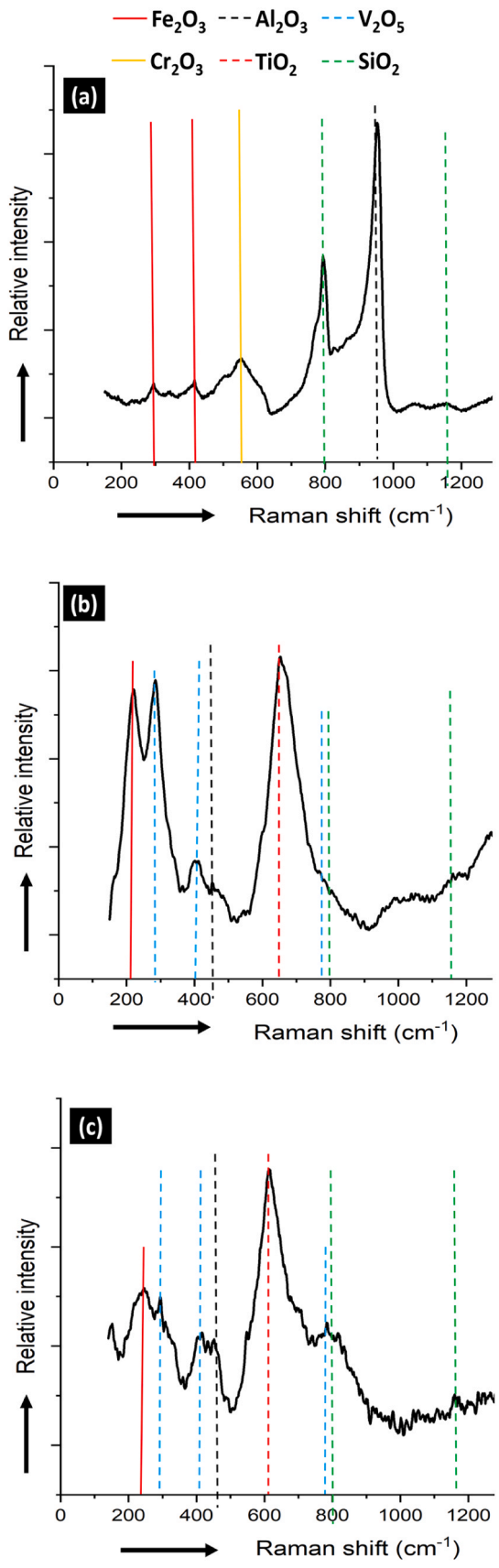


Fig. 12. Raman analysis conducted at the oxidation zone for (a) Al_2O_3/SiC uncoated, (b) TiAlSiV5N coated, and (c) TiAlSiV11N coated tools.

compared, the TiAlSiVN coated tools exhibit remarkable decrease in overall surface roughness with TiAlSiV5N and TiAlSiV11N coated tools showing an approximate maximum decrease in surface roughness of 60% and 66% respectively (see Fig. 6(b)). The percentage decrease in surface roughness decreases with cutting speed for the coated tools. Although, TiAlSiV11N coated tool showed an increase in percentage reduction which may be attributed to the lower friction and higher V content resulting in more lubricious phases in the cutting zone.

3.4. Cutting temperature

The measured cutting temperatures for each pass at the cutting zone have been plotted against cutting speed for TiAlSiVN coated and uncoated cutting tools in Fig. 7. The cutting temperature increases for all the cutting tools till 300 m/min cutting speed. However, at 350 m/min cutting speed, the cutting temperatures decrease due to severe thermal softening causing ease of material removal from the workpiece. Also, higher tool wear causes a loss of[33] effective cutting edge which can also be a cause of reduced cutting temperatures. Further, the change in cutting temperature between passes shown in Fig. 8(a) is not very high, basically due to the combined effect of thermal softening and subsequent work hardening developed due to the machining-induced stresses [34]. Also, TiAlSiVN coated tools results in reduction of cutting temperatures basically due to lower friction. However, this reduction decreases with increase of cutting speed (see Fig. 8(b)) indicating diminishing of favourable lubrication offered by coated tools with cutting speed.

3.5. Crater wear

The crater wear was observed using optical microscopy during each pass for both the TiAlSiVN coated and uncoated cutting tools. However, the abrasive crater wear was on the lower side for both uncoated and coated tools with only significant effect on the tool face being the adhesion wear. Thus, the tool wear on the rake surface has been elaborated using SEM images of the rake surface at the maximum cutting speed of 350 m/min. The crater wear has been categorized in two different zones: Zone 1 representing a region near the cutting edge which is basically formed due to abrasion and Zone 2 formed due to contact of tool and the chips accounting to adhesion. In this regard, Fig. 9 illustrates the SEM micrographs showing wear on the rake surface of Al_2O_3/SiC uncoated cutting tool after machining at 350 m/min cutting speed. The wear in Zone 1 is characterized by abrasion and severe adhesion and oxidation of workpiece material which is evident from the EDS elemental mapping shown in Fig. 9(e). There is layered deposition of the workpiece material on the tool face. The movement of chips on this layered deposition led to the attrition of the tool material which can be seen in form of tool fragments in Zone 1. In Zone 2, the wear is characterized by chip sticking, adhesion, and formation of lamellar debris.

On the contrary, for the TiAlSiV5N coated tool, the wear in Zone 1 (see Fig. 10) is less severe in terms of adhesion and the tool is clearly visible, which is also evident from the elemental mapping shown in Fig. 10(e). Although, a complete delamination of coating is seen in Zone 1, the edges of Zone 1 clearly indicate more gradual abrasive wear on the coating surface. Further, the size of Zone 1 is also reduced due to the deposition of TiAlSiV5N coating. It is evident that coating delamination is the main cause of coating failure, however, adhesion and chip sticking in Zone 2 for TiAlSiV5N coated tool are minimal illustrating superior anti-adhesive properties for the coating when compared to the Al_2O_3/SiC tool material. Additionally, the EDS elemental mapping shows signs of oxidation of coating and tool material.

When the wear in Zone 1 for the TiAlSiV11N coated tool (see Fig. 11) is analysed, not only the adhesion is on the lower side but also the size of Zone 1 is smaller when compared to the TiAlSiV5N coating. The increase in V content has shown improvement in frictional behaviour in the cutting zone which is reflected in the wear behaviour on the rake

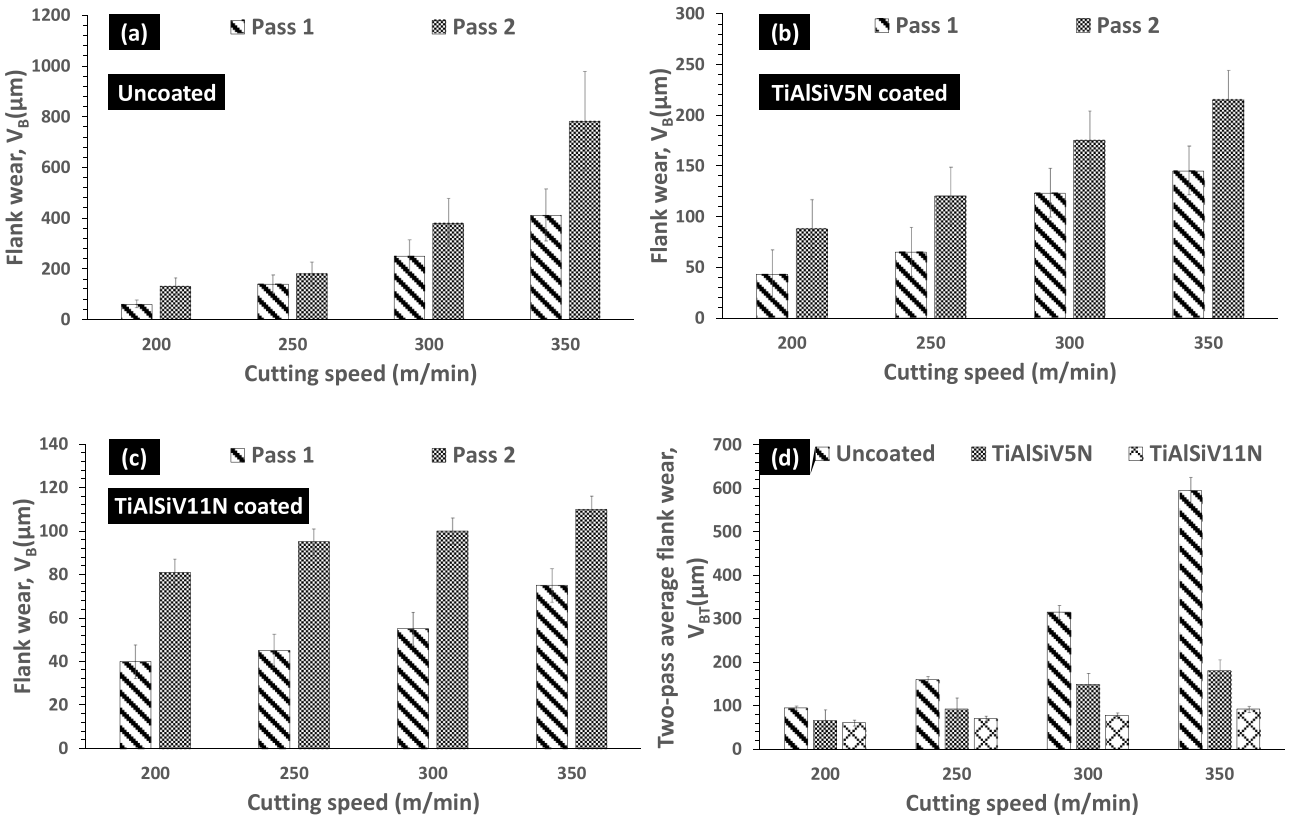


Fig. 13. Variation of flank wear with cutting speed for (a) Al_2O_3/SiC uncoated, (b) TiAlSiV5N coated, and (c) TiAlSiV11N coated tools for two passes. (d) Variation of two-pass average flank wear with cutting speed.

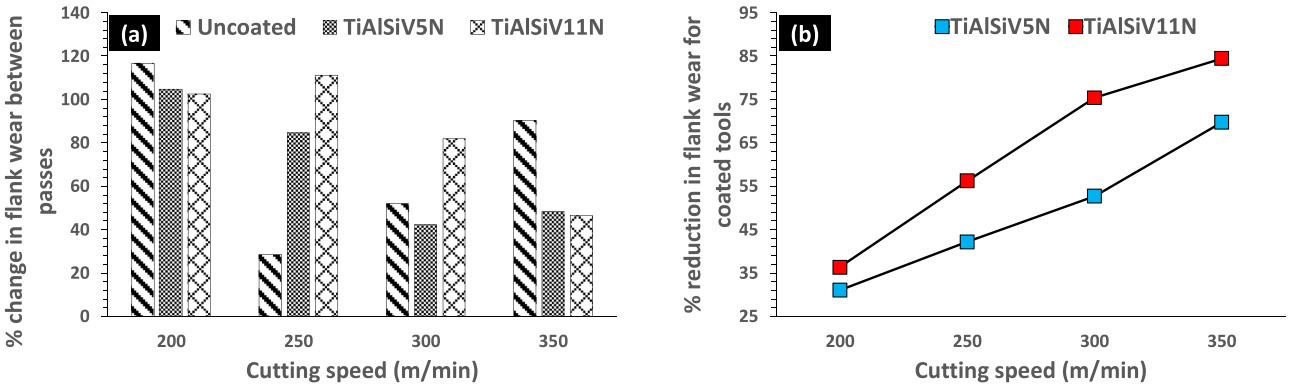


Fig. 14. Variation with cutting speed in (a) percentage (%) change in flank wear between passes and (b) percentage (%) reduction in flank wear for coated tools.

surface. Further, coating delamination has reduced basically due to superior coating/substrate adhesion strength for coating with 11% V. In Zone 2, the adhesion is even lower than the TiAlSiV5N coated tool. Further, like TiAlSiV5N coated tool, the EDS elemental mapping shown in Fig. 11(e) displays signs of oxidation of coating and tool material.

3.6. Raman analysis

The oxides formed on the top of the tool and coating material has been further investigated through Raman spectroscopy which has been shown in Fig. 12. The phases marked in the plotted spectrum have been identified from already published literature [35–41]. In the spectrum of uncoated tool, the presence of Fe_2O_3 and Cr_2O_3 indicate oxidation of workpiece material whereas, the presence of SiO_2 indicate the oxidation of tool material. Similarly, for the coated tools, the presence of Fe_2O_3 indicates the oxidation of workpiece material, and the presence of TiO_2, SiO_2, and V_2O_5 indicates the oxidation of tool and coating material. Both coated tools show the presence of V_2O_5 in the cutting zone, which is reported to be a self-lubricant phase beneficial for reducing friction [42, 43]. Thus, it is evident from the Raman analysis that the generation of V_2O_5 lubricious phase in the cutting zone helps to reduce friction, as reported in Section 3.2.

3.7. Flank wear

The measured flank wear has been plotted against cutting speed in Fig. 13. Also, the progression of flank wear between passes has been plotted. The flank wear increases with cutting speed for all the cutting tools. Evidently, a growth of flank wear is seen in the second pass showing its progressive increase over time. Interestingly, the fluctuation

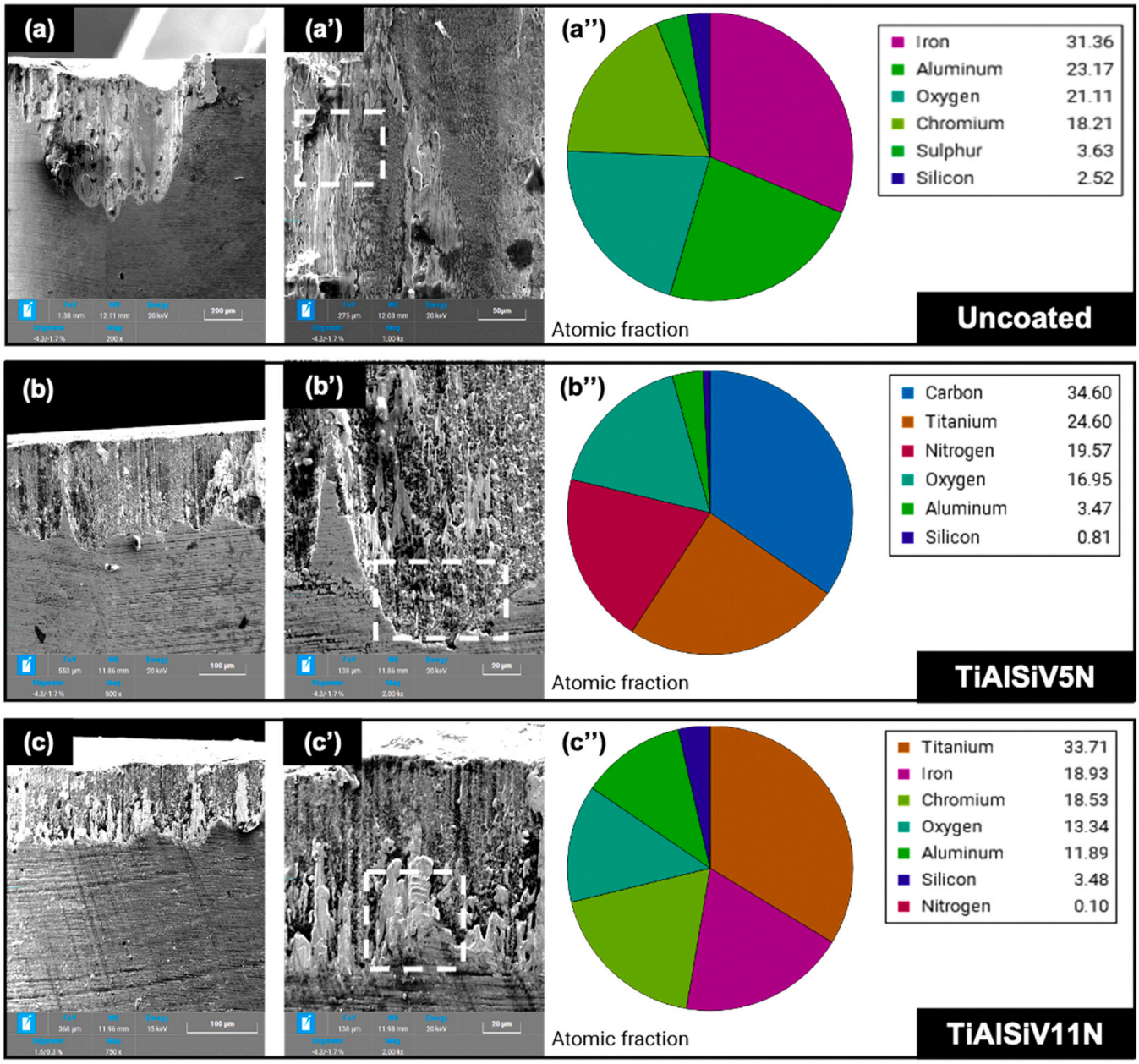


Fig. 15. SEM micrographs showing flank wear on (a) Al_2O_3/SiC uncoated, (b) TiAlSiV5N coated, and (c) TiAlSiV11N coated tools after machining at 350 m/min cutting speed.

of flank wear is on the lower side for the TiAlSiV11N coated tool, basically due to the reduction in friction offered by the coating, which accounts for lower fluctuations in machining forces during the cutting operation. Further, the coated tools have shown a significant flank wear reduction when compared to the uncoated tool with TiAlSiV11N coating, showing the maximum reduction (see Fig. 13(d)). Further, the percentage change in flank wear shown in Fig. 14(a) is random over passes and does not follow any trend. However, the percentage reduction in flank wear (see Fig. 14(b)) offered by the TiAlSiVN coated tools increases with increase of cutting speed. The increase of temperature with cutting speed may be one of the reasons leading to elevated oxidation of coating and higher V_2O_5 lubrication phases in the cutting zone. The higher lubricious phases in the cutting zone reduce friction and, thus, improve the amount of flank wear reduction for coated tools. For the same reason, coating with 11% V content accounts for more flank wear reduction (a maximum of approx. 85%) and generation of more lubricious phases in the cutting zone when compared to the coating with 5% V content (a maximum of approx. 67%).

The flank wear study has been further elaborated through SEM images of the flank surface after machining at 350 m/min cutting speed in Fig. 15. The flank wear on the cutting tools is characterized by adhesion and abrasion. Alike wear on the rake surface, the adhesion on the coated tools is on the lower side. Additionally, on the uncoated tool, abrasion leads to chipping towards the cutting edge.

4. Conclusions

In the present work, the effect of V content on the performance of TiAlSiVN coating during dry machining of austenitic 316 L steel has been investigated. The presented results lead to the following conclusions:

1. The variation in cutting force over subsequent passes in minimal. However, the TiAlSiV11N coated tool accounted to lower

fluctuations in the cutting forces basically due to reduced friction when compared to the uncoated and TiAlSiV5N coated tool. Machining with TiAlSiVN coated tool led to noticeable reduction in surface roughness values when compared to the uncoated tool. For TiAlSiV11N coated tool, the change in surface roughness over subsequent passes was negligible till 300 m/min cutting speed and then, it increases at 350 m/min indicating higher tool wear.

2. TiAlSiVN coated tools result in reduction of cutting temperatures basically due to lower friction. However, this reduction decreases with increase of cutting speed indicating diminishing of favourable lubrication offered by coated tools with cutting speed.
3. The deposition of TiAlSiVN coating on the cutting tools prevented not only severe adhesion near the cutting edge but also fragmentation of tool material due to attrition in Zone 1. Whereas in Zone 2, coated tools exhibited minimal chip sticking and adhesion. TiAlSiV11N coating accounted to lower coating delamination when compared to the TiAlSiV5N coating owing to its better coating/substrate adhesion strength.
4. Raman analysis shows the presence of Fe_2O_3 and Cr_2O_3 indicating oxidation of workpiece material, whereas the presence of TiO_2, SiO_2 and V_2O_5 represents oxidation of tool and coating material. The presence of V_2O_5 proves the lubricous effect produced by the TiAlSiVN coating during the machining operation.
5. The higher the lubricious phases in the cutting zone, the lower the friction. Therefore, coating with 11% V content accounts to a maximum flank wear reduction of 85% when compared to the 67% reduction offered by coating with 5% V content.

Statement of Originality

As a corresponding author of the paper, I hereby declare that the work has not been published elsewhere and is not under review with any other journals.

CRediT authorship contribution statement

Fernandes Filipe: Funding acquisition, Formal analysis, Data curation. **Rjoub Abbas AL:** Data curation. **De Lacalle Luis Norberto López:** Resources, Funding acquisition. **Kumar Ch Sateesh:** Validation, Methodology, Investigation, Formal analysis, Data curation, Conceptualization. **Urbikain Gorka:** Supervision.

Declaration of Competing Interest

The authors declare that they have no known competing financial interests or personal relationships that could have appeared to influence the work reported in this paper.

Data availability

Data will be made available on request.

Acknowledgements

The work is supported by Maria Zambrano grants. Thanks are addressed to project PDC2021–121792-I00 (HCR Taylor) funded by MCIN/AEI /10.13039/501100011033 and by European Union Next Generation EU/ PRTR and Project NEOFHYM (PID2022–137380OB-I00) MCIN/ AEI /10.13039/501100011033. The authors also thank SGIker (UPV/EHU/ ERDF, EU) for technical and human support. This research is also sponsored by FEDER Funds through Portugal 2020 (PT2020), by the Competitiveness and Internationalization Operational Program (COMPETE 2020), and national funds through the Portuguese Foundation for Science and Technology (FCT) under the projects: MCTool21-ref:" POCI-01–0247-FEDER-045940", UIDB/00285/2020 and LA/P/0112/2020.

References

[1] Pang X, Zhang B, Li S, Zeng Y, Liu X, Shen P, Li Z, Deng W. Machining performance evaluation and tool wear analysis of dry cutting austenitic stainless steel with variable-length restricted contact tools. Wear 2022;504–505:204423. https://doi.org/10.1016/j.wear.2022.204423.
[2] Nur R, Noordin MY, Izman S, Kurniawan D. Machining parameters effect in dry turning of AISI 316L stainless steel using coated carbide tools. Proc Inst Mech Eng, Part E: J Process Mech Eng 2017;231:676–83. https://doi.org/10.1177/0954408915624861.
[3] Das CR, Ghosh A. Performance of carbide end mills coated with new generation nano-composite TiAlSiN in machining of austenitic stainless steel under near-dry (MQL) and flood cooling conditions. J Manuf Process 2023;104:418–42. https://doi.org/10.1016/j.jmapro.2023.09.020.
[4] Bartarya G, Choudhury SK. State of the art in hard turning. Int J Mach Tools Manuf 2012;53:1–14. https://doi.org/10.1016/j.ijmachtools.2011.08.019.
[5] Eltaggaz A, Nouzil I, Deiab I. Machining ti-6al-4v alloy using nano-cutting fluids: investigation and analysis. J Manuf Mater Process 2021;5. https://doi.org/10.3390/jmmp5020042.
[6] Rech J. Influence of cutting tool coatings on the tribological phenomena at the tool-chip interface in orthogonal dry turning. Surf Coat Technol 2006;200:5132–9. https://doi.org/10.1016/j.surfcoat.2005.05.032.
[7] Nouari M, Ginting A. Wear characteristics and performance of multi-layer CVD-coated alloyed carbide tool in dry end milling of titanium alloy. Surf Coat Technol 2006;200:5663–76. https://doi.org/10.1016/j.surfcoat.2005.07.063.
[8] Maruda RW, Krolczyk GM, Feldshtein E, Nieslony P, Tyliszczak B, Pusavec F. Tool wear characterizations in finish turning of AISI 1045 carbon steel for MQCL conditions. Wear 2017;372–373:54–67. https://doi.org/10.1016/j.wear.2016.12.006.
[9] El Hakim MA, Abad MD, Abdelhameed MM, Shalaby MA, Veldhuis SC. Wear behavior of some cutting tool materials in hard turning of HSS. Tribol Int 2011;44:1174–81. https://doi.org/10.1016/j.triboint.2011.05.018.
[10] Aslantas K, Ucun TI, çicek A. Tool life and wear mechanism of coated and uncoated Al2O3/TiCN mixed ceramic tools in turning hardened alloy steel. Wear 2012;274–275:442–51. https://doi.org/10.1016/j.wear.2011.11.010.
[11] Barshilia HC, Ghosh M, Shashidhara, Ramakrishna R, Rajam KS. Deposition and characterization of TiAlSiN nanocomposite coatings prepared by reactive pulsed direct current unbalanced magnetron sputtering. Appl Surf Sci 2010;256:6420–6. https://doi.org/10.1016/j.apsusc.2010.04.028.
[12] Saketi S, Östby J, Olsson M. Influence of tool surface topography on the material transfer tendency and tool wear in the turning of 316L stainless steel. Wear 2016;368–369:239–52. https://doi.org/10.1016/j.wear.2016.09.023.
[13] Wang SQ, Chen L, Yang B, Chang KK, Du Y, Li J, Gang T. Effect of Si addition on microstructure and mechanical properties of Ti-Al-N coating. Int J Refract Met Hard Mater 2010;28:593–6. https://doi.org/10.1016/j.ijrmhm.2010.05.001.
[14] Veprek S, M??nnling HD, Jilek M, Holubar P. Avoiding the high-temperature decomposition and softening of (Al1-xTix)N coatings by the formation of stable superhard nc-(Al1-xTix)N/a-Si3 N4 nanocomposite. Mater Sci Eng A 2004;366:202–5. https://doi.org/10.1016/j.msea.2003.08.052.
[15] Holubář P, Jílek M, Šíma M. Nanocomposite nc-TiAlSiN and nc-TiN-BN coatings: their applications on substrates made of cemented carbide and results of cutting tests. Surf Coat Technol 1999;120–121:184–8. https://doi.org/10.1016/S0257-8972(99)00483-1.
[16] Kumar CS, Patel SK. Performance analysis and comparative assessment of nano-composite TiAlSiN/TiSiN/TiAlN coating in hard turning of AISI 52100 steel. Surf Coat Technol 2018;335:265–79. https://doi.org/10.1016/j.surfcoat.2017.12.048.
[17] Brzezinka T, Rao J, Paiva J, Kohlscheen J, Fox-Rabinovich G, Veldhuis S, Endrino J. DLC and DLC-WS2 Coatings for Machining of Aluminium Alloys. Coatings 2019;9:192. https://doi.org/10.3390/coatings9030192.
[18] Kumar CS, Urbikain G, De Lucio PF, De Lacalle LNL, Pérez-Salinas C, Gangopadhyay S, Fernandes F. Investigating the self-lubricating properties of novel TiSiVN coating during dry turning of Ti6Al4V alloy. Wear 2023;532–533. https://doi.org/10.1016/j.wear.2023.205095.
[19] Çomakli O, Yetim T, Çelik A. The effect of calcination temperatures on wear properties of TiO2 coated CP-Ti. Surf Coat Technol 2014;246:34–9. https://doi.org/10.1016/j.surfcoat.2014.02.059.
[20] Fernandes F, Oliveira JC, Cavaleiro A. Self-lubricating TiSi(V)N thin films deposited by deep oscillation magnetron sputtering (DOMS). Surf Coat Technol 2016;308:256–63. https://doi.org/10.1016/j.surfcoat.2016.07.039.
[21] Wang SQ, Chen L, Yang B, Chang KK, Du Y, Li J, Gang T. Effect of Si addition on microstructure and mechanical properties of Ti-Al-N coating. Int J Refract Met Hard Mater 2010;28:593–6. https://doi.org/10.1016/j.ijrmhm.2010.05.001.
[22] Calıskan H, Kurbanoglu C, Panjan P, Cekada M, Kramar D. Wear behavior and cutting performance of nanostructured hard coatings on cemented carbide cutting tools in hard milling. Tribol Int 2013;62:215–22. https://doi.org/10.1016/j.triboint.2013.02.035.
[23] Kumar CS, Patel SK. Effect of duplex nanostructured TiAlSiN/TiSiN/TiAlN-TiAlN and TiAlN-TiAlSiN/TiSiN/TiAlN coatings on the hard turning performance of Al 2 O 3 -TiCN ceramic cutting tools. Wear 2019;418–419:226–40. https://doi.org/10.1016/j.wear.2018.11.013.
[24] Li G, Sun J, Xu Y, Xu Y, Gu J, Wang L, Huang K, Liu K, Li L. Microstructure, mechanical properties, and cutting performance of TiAlSiN multilayer coatings prepared by HiPIMS. Surf Coat Technol 2018;353:274–81. https://doi.org/10.1016/j.surfcoat.2018.06.017.

[25] Kumar CS, Patel SK. Performance analysis and comparative assessment of nano-composite TiAlSiN/TiSiN/TiAlN coating in hard turning of AISI 52100 steel. Surf Coat Technol 2018;335:265–79. https://doi.org/10.1016/j.surfcoat.2017.12.048.
[26] Das P, Anwar S, Bajpai S, Anwar S. Structural and mechanical evolution of TiAlSiN nanocomposite coating under influence of Si3N4 power. Surf Coat Technol 2016; 307:676–82. https://doi.org/10.1016/j.surfcoat.2016.09.065.
[27] Al-rjoub A, Bin T, Cavaleiro A, Fernandes F. The influence of V addition on the structure, mechanical properties, and oxidation behaviour of TiAlSiN coatings deposited by DC magnetron sputtering. J Mater Res Technol 2022;20:2444–53. https://doi.org/10.1016/j.jmrt.2022.08.009.
[28] Fukuyama H, Higashi H, Yamano H. Normal spectral emissivity, specific heat capacity, and thermal conductivity of type 316 austenitic stainless steel containing up to 10 mass% B4C in a liquid state. J Nucl Mater 2022;568:153865. https://doi.org/10.1016/j.jnucmat.2022.153865.
[29] Özel T. The influence of friction models on finite element simulations of machining. Int J Mach Tools Manuf 2006;46:518–30. https://doi.org/10.1016/j.ijmachtools.2005.07.001.
[30] Grzesik W, Zak K. Friction quantification in the oblique cutting with CBN chamfered tools. Wear 2013;304:36–42. https://doi.org/10.1016/j.wear.2013.04.020.
[31] Ding H, Zou B, Wang X, Liu J, Li L. Microstructure, mechanical properties and machinability of 316L stainless steel fabricated by direct energy deposition. Int J Mech Sci 2023;243:108046. https://doi.org/10.1016/j.ijmecsci.2022.108046.
[32] Kumar CS, Patel SK. Effect of chip sliding velocity and temperature on the wear behaviour of PVD AlCrN and AlTiN coated mixed alumina cutting tools during turning of hardened steel. Surf Coat Technol 2017;334:509–25. https://doi.org/10.1016/j.surfcoat.2017.12.013.
[33] Debnath S, Reddy MM, Yi QS. Influence of cutting fluid conditions and cutting parameters on surface roughness and tool wear in turning process using Taguchi method. Meas (Lond) 2016;78:111–9. https://doi.org/10.1016/j.measurement.2015.09.011.
[34] O'Sullivan D, Cotterell M. Machinability of austenitic stainless steel SS303. J Mater Process Technol 2002;124:153–9. https://doi.org/10.1016/S0924-0136(02)00197-8.
[35] Col A, Parry V, Pascal C. Oxidation of a Fe–18Cr–8Ni austenitic stainless steel at 850 °C in O2: Microstructure evolution during breakaway oxidation. Corros Sci 2017;114:17–27. https://doi.org/10.1016/j.corsci.2016.10.029.
[36] Hardcastle FD, Wachs IE. Raman spectroscopy of chromium oxide supported on Al2O3, TiO2 and SiO2: a comparative study. J Mol Catal 1988;46:173–86. https://doi.org/10.1016/0304-5102(88)85092-2.
[37] Kobayashi T, Hirajima T, Hiroi Y, Svojtka M. Determination of SiO2 raman spectrum indicating the transformation from coesite to quartz in Gföhl migmatitic gneisses in the Moldanubian Zone, Czech Republic. J Mineral Petrol Sci 2008;103:105–11. https://doi.org/10.2465/jmps.071020.
[38] Fernandes F, Morgiel J, Polcar T, Cavaleiro A. Oxidation and diffusion processes during annealing of TiSi(V)N films. Surf Coat Technol 2015;275:120–6. https://doi.org/10.1016/j.surfcoat.2015.05.031.
[39] Zhang WF, He YL, Zhang MS, Yin Z, Chen Q. Raman scattering study on anatase TiO2 nanocrystals. J Phys D Appl Phys 2000;33:912–6. https://doi.org/10.1088/0022-3727/33/8/305.
[40] Su Q, Huang CK, Wang Y, Fan YC, Lu BA, Lan W, Wang YY, Liu XQ. Formation of vanadium oxides with various morphologies by chemical vapor deposition. J Alloy Compd 2009;475:518–23. https://doi.org/10.1016/j.jallcom.2008.07.078.
[41] F. Gyakwaa, T. Alatarvas, Q. Shu, M. Aula, T. Fabritius, Characterization of Synthetic Non-Metallic Inclusions, (2021).
[42] Ponomarev I, Polcar T, Nicolini P. Tribological properties of V2O5 studied via reactive molecular dynamics simulations. Tribol Int 2021;154:106750. https://doi.org/10.1016/j.triboint.2020.106750.
[43] Mirabal-Rojas R, Rodil SE, Ramirez G, Polcar T, Camps E, Erdemir A. Effect of the addition of Si into V2O5 coatings: structure and tribo-mechanical properties. Surf Coat Technol 2018;349:111–8. https://doi.org/10.1016/j.surfcoat.2018.05.052.